Applied Catalysis B: Environmental 110 (2011) 154–163

Contents lists available at SciVerse ScienceDirect

Applied Catalysis B: Environmental

journal homepage: www.elsevier.com/locate/apcatb

Mesoporous ceria-zirconia supported cobalt oxide catalysts for CO preferential oxidation reaction in excess H_2

Zhongkui Zhao[a,*], Ronghua Jin[a], Ting Bao[a], Xiaoli Lin[a], Guiru Wang[b]

[a] State Key Laboratory of Fine Chemicals, Department of Fine Chemicals, School of Chemical Engineering, Dalian University of Technology, 2 Linggong Road, Dalian 116024, China
[b] Department of Catalytic Chemistry and Engineering, School of Chemical Engineering, Dalian University of Technology, 2 Linggong Road, Dalian 116024, China

ARTICLE INFO

Article history:
Received 25 May 2011
Received in revised form 13 July 2011
Accepted 30 August 2011
Available online 3 September 2011

Keywords:
Mesoporous ceria-zirconia composite
Cobalt oxide loading
Structure-directing agent
Ce/(Ce + Zr) atomic ratio
CO preferential oxidation

ABSTRACT

Mesoporous $Co_3O_4/Ce_xZr_{1-x}O_2$ (x = 0.75, 0.85, 0.95, 1) catalysts were synthesized by surfactant-assisted co-precipitation with subsequent incipient wetness impregnation (SACP-IWI) method. The prepared mesoporous ceria-zirconia supported cobalt oxide catalysts were used to catalyze CO preferential oxidation (PROX) reaction to eliminate the trace CO from H_2-rich gases. The effects of structure-directing agent (SDA) type, atomic ratio of Ce/(Ce + Zr), cobalt oxide loading and reaction parameters on the catalytic properties for CO PROX reaction in excess H_2 were investigated. Moreover, the various characterization techniques like N_2 adsorption/desorption, X-ray diffraction (XRD), H_2 temperature-programmed reduction (H_2-TPR), NH_3 temperature-programmed desorption (NH_3-TPD), Fourier-Transform infrared spectroscopy (FT-IR) were employed to study the relationship between catalyst nature and catalytic properties. The results of N_2 adsorption/desorption and X-ray diffraction patterns indicate that catalysts prepared by using cationic surfactant cetyltrimethylammonium bromide (CTAB) as SDA possess an ordered mesoporous architecture and exhibit much better catalytic activity compared with those prepared by using anionic surfactant ammonium dodecylbenzenesulfonate (ADBS) as SDA. The residual sulfur from ADBS was demonstrated to be the main reason for the much worse catalytic performance by the characterization results of FT-IR and NH_3-TPD. Results show that the developed Co_3O_4/*meso*-$Ce_{0.85}Zr_{0.15}O_2$ catalysts by SACP-IWI method with CTAB as SDA show an outstanding catalytic performance for CO PROX reaction, which mainly depends on the redox behavior of catalyst and cobalt oxide dispersion affected by the ceria-zirconia support feature, atomic ratio of Ce/(Ce + Zr) of support and cobalt oxide loading.

1. Introduction

Proton exchange membrane fuel cells (PEMFCs) have become the most attractive clean alternatives to conventional combustion of fossil fuels to generate energy with high efficiency and power density but low operating temperature [1–4]. The hydrogen used in PEMFCs generally comes from reforming streams of hydrocarbon and alcohols, which may still contain 0.5–2% CO even after undergoing the high and subsequent low temperature water-gas shift (WGS) reactions. However, the trace amount of CO can easily poison the anode materials of PEMFCs. The allowed CO concentrations are defined as less than 10 ppm for a Pt anode and less than 100 ppm for a CO-tolerant alloy anode [5,6]. Therefore, various strategies have been developed to remove the trace amount of CO from the H_2-rich gases. Among them, the CO PROX reaction has been considered as the simplest and most effectual method for purifying H_2-rich gases. The key point of this method is to find catalysts having good activity and selectivity for CO oxidation in the presence of H_2 at a wide temperature-window, high tolerance towards CO_2 and H_2O those exist in the reformed fuel, but low activity for the undesired side reactions like H_2 oxidation, reverse WGS, methanization, etc.

Catalysts reported for CO PROX reactions are mainly precious metal catalysts, such as Au, Pt, Ru and Rh, exhibiting better low-temperature activity in comparison with base metal catalysts [7–12]. Due to the high cost and limited availability of precious metals, the catalysts based on non-precious metals are considered as promising alternatives for CO PROX reaction in excess H_2. CuO-CeO_2 [13–15] and CuO/CeO_2 [16,17] systems, especially, were well studied and the good catalytic performance for CO PROX reaction had been achieved. Nowadays, many reports focus on Cu based catalysts for CO PROX reaction, and have achieved fruitful results. But some shortcomings such as less anti-H_2O, CO_2 capability, not satisfactory CO selectivity and also narrow temperature window, etc. remain to be overcome. Studies on the other non-precious metals gain increasing attentions. Co based catalysts with outstanding catalytic properties have shown better low-temperature activity,

* Corresponding author. Tel.: +86 411 84986231; fax: +86 411 84986231.
E-mail address: zkzhao@dlut.edu.cn (Z. Zhao).

0926-3373/$ – see front matter © 2011 Elsevier B.V. All rights reserved.
doi:10.1016/j.apcatb.2011.08.038

selectivity and the H_2O resistance than CuO_x, which can be considered as a promising candidate for the CO PROX reaction in excess H_2 [18–23]. Co^{3+} as the active site provides its lattice-oxygen to the CO ultimately forming a Co^{2+} that can be re-oxidized with oxygen [20,24]. While during the CO PROX process, the H_2 in feed gets high-valence cobalt reduced to low-valence ones [25,26], which is not active for CO PROX reaction. Supported on a metal oxide carrier is a feasible way for Co^{3+} to be kept at its high-valence state in a H_2 atmosphere [27]. The support materials could essentially play a significant role in modifying the formation of active Co metal species via metal–support interaction. Many reports have shown that the supported cobalt catalysts possess excellent redox behaviors [28–31]. The CeO_2-ZrO_2 composite oxide system, for its peculiar optical and magnetic properties and especially the unexpected oxygen mobility, has been supposed to be a candidate for support to stabilize the high-valence cobalt species. In our previous studies [32], cobalt oxide supported on CeO_2-ZrO_2 nanoparticle showed promising catalytic performance for CO PROX reaction in the presence of H_2. Nevertheless, the low specific surface area of nanoparticle as support is its essential limitation, which is unfavorable for the dispersion of active species. To prepare ceria-zirconia composite oxide with mesoporous structure is an efficient avenue to enlarge its specific surface area. Moreover, the morphologies have been found to significantly affect the oxygen vacancy formation energy of support, resulting in different catalytic properties [16]. Herein, we prepared the different mesoporous ceria-zirconia composite oxides by SACP method with two kinds of SDA (CTAB and ADBS), and then supported cobalt oxide to obtain a series of Co_3O_4/*meso*-$Ce_xZr_{1-x}O_2$ catalysts. The effects of SDA (cationic and anionic surfactant), Ce/(Ce + Zr) atomic ratio and cobalt oxide loading amount on the catalyst nature and the catalytic performance for CO PROX reaction in excess H_2 were investigated. In addition, the influence of reaction parameters like CO_2 and H_2O in the feed, gas hourly space velocity (GHSV) and O_2 concentration on CO PROX reaction was also investigated. Characterizations including XRD, N_2 adsorption/desorption, FT-IR, H_2-TPR and NH_3-TPD were employed to investigate the relationship between physicochemical properties of catalysts and catalytic performance. In the present paper, we find out that the prepared catalysts employing CTAB as SDA possess ordered mesoporous architecture and show promising catalytic performance for CO PROX reaction in excess H_2. However, the supported cobalt oxide catalyst with ceria-zirconia as support using the ADBS as SDA owns much worse activity for CO PROX reaction. The negative effect of anionic ADBS as SDA was found to be mainly corroborated to the residual sulfur, which gives an acidic nature to catalyst that is apt to break the equilibrium of surface acidic and basic sites, resulting in very low activity for CO oxidation. The prepared Co_3O_4/*meso*-$Ce_xZr_{1-x}O_2$ (CTAB as SDA) could be effective catalysts for eliminating CO from H_2-rich gases, and the catalytic performance is dependent on the redox behavior and Co_3O_4 dispersion, affected by the Ce/(Ce + Zr) ratio and cobalt oxide loading.

2. Experimental

2.1. Catalysts preparation

The $Ce_xZr_{1-x}O_2$ (x = 0.75, 0.85, 0.95, 1) composite oxides were prepared by the SACP method. Typically, 17 mmol of ammonium cerium nitrate (Sinopharm, AR) and 3 mmol of zirconium nitrate (Tianjin Damao, AR) were dissolved in deionizied water. A certain amount of CTAB (Kermel, AR) was added to 25 ml of deionized water to give a clear homogeneous solution. Then, the two solutions were mixed under continuously stirring for 2 h. Afterward, pre-determined amount of ammonium solution (25%) was added drop by drop under vigorous stirring, leading to a final pH value of 11. After precipitation, the gelatinous pale yellow mixture was stirred for further 4 h and subsequently transferred to Teflon autoclaves, which were kept at 105–120 °C for 3 d. The solid product was filtered, washed with deionized water and ethanol, subsequently dried at 105 °C overnight, and then calcined in a muffle furnace in air with T_{sup} at 550 °C for 6 h, where T_{sup} was denoted as the calcination temperature for preparing mesoporous ceria-zirconia composite oxide supports. Preparation of the other $Ce_xZr_{1-x}O_2$ composite oxides with different Ce/(Ce + Zr) atomic ratios underwent the same way but only changing the relative amount of Ce and Zr precursors. $Ce_{0.85}Zr_{0.15}O_2$ composite oxide was also synthesized using ADBS as SDA.

The mesoporous $Co_3O_4/Ce_xZr_{1-x}O_2$ (x = 0.75, 0.85, 0.95, 1) catalysts with various cobalt loadings (4 wt.%, 8 wt.%, 12 wt.%, 16 wt.%, 20 wt.% and 27 wt.%) were prepared by IWI method using cobalt nitrate (Tianjin Bodi, AR) as Co precursor. After each impregnation step, the sample was dried at 105 °C for 2 h to evaporate the solvent, and the final sample was calcined at 450 °C in air for 5 h.

2.2. Catalysts characterization

The BET specific surface area, total pore volume and pore size distribution were obtained from the adsorption and desorption isotherms of nitrogen at −196 °C using a Quantachrome Autosorb-1 apparatus. FT-IR spectra were collected in the wave number range 4000–400 cm^{-1} on EQUINOX-55 Fourier Transform Infrared Spectrometer (BRUKER). The powder XRD experiments were carried out on Rigaku Automatic X-ray Diffractometer (D/Max 2400) equipped with a Cu Kα source (λ = 1.5406 Å). The XRD patterns were recorded from 0.5° to 80° with a step width of 0.02°. The crystallite parameters were estimated based the Scherrer Formula over multiple characteristic diffraction peaks by the MDI Jade5 software.

H_2-TPR experiments were performed in an in-house constructed system equipped with a thermal conductivity detector (TCD) to measure H_2 consumption. 50 mg sample was pretreated under a 2.5 vol.% O_2/Ar flow (30 ml min^{-1}) at 450 °C (the same as the calcination temperature for catalyst preparation) for 30 min, followed by cooling to room temperature in an Ar flow (30 ml min^{-1}). After that, it was reduced with a 10 vol.% H_2/Ar mixture (30 ml min^{-1}) by heating up to 800 °C at a ramp rate of 10 °C min^{-1}.

The acidic properties of the catalysts were measured by an in-house constructed system equipped with a thermal conductivity detector (TCD) to monitor desorbed NH_3. After pretreated with Ar at 450 °C (the same as the calcination temperature for catalyst preparation) for 30 min, the reactor was cooled down to about 150 °C, and then saturated with pulse introduction of NH_3. The sufficient saturation was checked by analyzing the outlet gas via a TCD. Afterwards, the sample was subjected to programmed-heating in an Ar flow with a ramp rate of 10 °C min^{-1}. Thermal desorption of NH_3 was recorded by TCD.

2.3. Catalytic performance tests

The catalytic activity tests for CO PROX reaction in H_2-rich gases were performed in a stainless steel, fixed bed continuous-flow reactor (6 mm O.D.) with 100–200 mg of catalyst held between two quartz wool plugs. The reaction feed consisted of 1.0 vol.% CO, 1.0 vol.% O_2, 50 vol.% H_2 and Ar balance. Samples were pretreated in 2.5 vol.% O_2/Ar flow at 300 °C for 30 min. The temperatures were measured by using K-type thermocouples and controlled by a PID controller. The analysis of the effluent gas was performed using a gas chromatograph on-line with a molecular sieve column and a Porapaq Q column. The CO and CO_2 signals were detected by the FID detector after the gas passing through a methanizer. 10 vol.%

CO_2 and/or 10 vol.%H_2O were added to the feed to simulate the reforming gas. The concentration of O_2 was changed from 1.0 to 1.25 vol.% to study the influence of O_2 concentration on the catalytic performance. The effect of gas hourly space velocity (GHSV) was investigated through changing the total flow rate of the feed from 7500 to 15,000 ml h^{-1} g^{-1}. The stability of the 20 wt.% Co_3O_4/*meso*-$Ce_{0.85}Zr_{0.15}O_2$ catalyst was investigated by performing a second run over the used catalyst. Both the CO conversion and the CO_2 selectivity were determined by the CO and O_2 concentrations in the feed and the effluent $[CO]_{in}$, $[CO]_{out}$, $[O_2]_{in}$ and $[O_2]_{out}$. CO conversion and CO_2 selectivity (O_2 selectivity to CO_2) were calculated on the basis of the equations as follows:

$$\text{CO Conversion } \chi_{CO}(\%) = \frac{[CO]_{in} - [CO]_{out}}{[CO]_{in}} \times 100$$

$$\text{O}_2 \text{ Conversion } \chi_{O_2}(\%) = \frac{[O_2]_{in} - [O_2]_{out}}{[O_2]_{in}} \times 100$$

$$\text{CO}_2 \text{ Selectivity } S_{CO_2}(\%) = \frac{\chi_{CO}}{2 \times \chi_{O_2}} \times 100$$

3. Results and discussion

3.1. Effect of structure-directing agent

The using of different SDA may change the morphology and surface area of sample, resulting in different catalytic performance that is dependent on the dispersion of the active component and the oxygen vacancies [33]. Generally, the used SDA in preparing mesoporous metal oxides are almost cationic surfactants, but the anionic surfactants are rarely adopted. Therefore, we prepared the *meso*-$Ce_{0.85}Zr_{0.15}O_2$ composite oxides by using CTAB and ADBS as SDA, and supported cobalt oxide on the mesoporous ceria-zirconia to obtain the two Co_3O_4/*meso*-$Ce_{0.85}Zr_{0.15}O_2$ catalysts, denoted as CTAB-550 and ADBS-550, respectively. The catalytic performance of the catalysts for CO PROX reaction is shown in Fig. 1.

From Fig. 1, CO conversion on ADBS-550 is definitely different from that on CTAB-550. The complete CO conversion over CTAB-550 at 165–200 °C can be observed. However, the CO PROX reaction can hardly take place on ADBS-550 (the CO_2 selectivity is random due to the ultralow CO conversion, not shown here). In consideration of the same preparation procedure for the two catalysts except for the type of SDA, we can suppose the residual sulfur from ADBS might be responsible for the inactivity of ADBS-550 catalyst. In addition, textural imparity resulted from the different SDA may be another reason. To identify the assumptions, the *meso*-$Ce_{0.86}Zr_{0.15}O_2$ support synthesized by ADBS was further treated with T_{sup} at 700 °C for 5 h before being impregnated with cobalt nitrate (the supported Co catalyst was denoted as ADBS-700). The CO conversion and CO_2 selectivity on the ADBS-700 are also presented in Fig. 1. Compared with ADBS-550, ADBS-700 catalyst demonstrates much better catalytic performance for CO PROX reaction (92% CO conversion and 46% CO_2 selectivity at 225 °C). It is generally accepted that the calcination at higher temperature would lead to the decrease in surface area, which is detrimental to the dispersion of cobalt oxide. However, the dramatically improved catalytic activity of supported cobalt oxide catalyst can be observed over ADBS-700, although the support was suffered from the further calcination process at high temperature of 700 °C. N_2 adsorption/desorption and XRD techniques were employed to prove the above hypothesis. Fig. 2 presents the N_2 adsorption/desorption isotherms and pore size distributions. The XRD patterns of these samples are shown in Figs. 3 and 4. The corresponding analysis data for N_2 adsorption/desorption and XRD patterns are listed in Table 1.

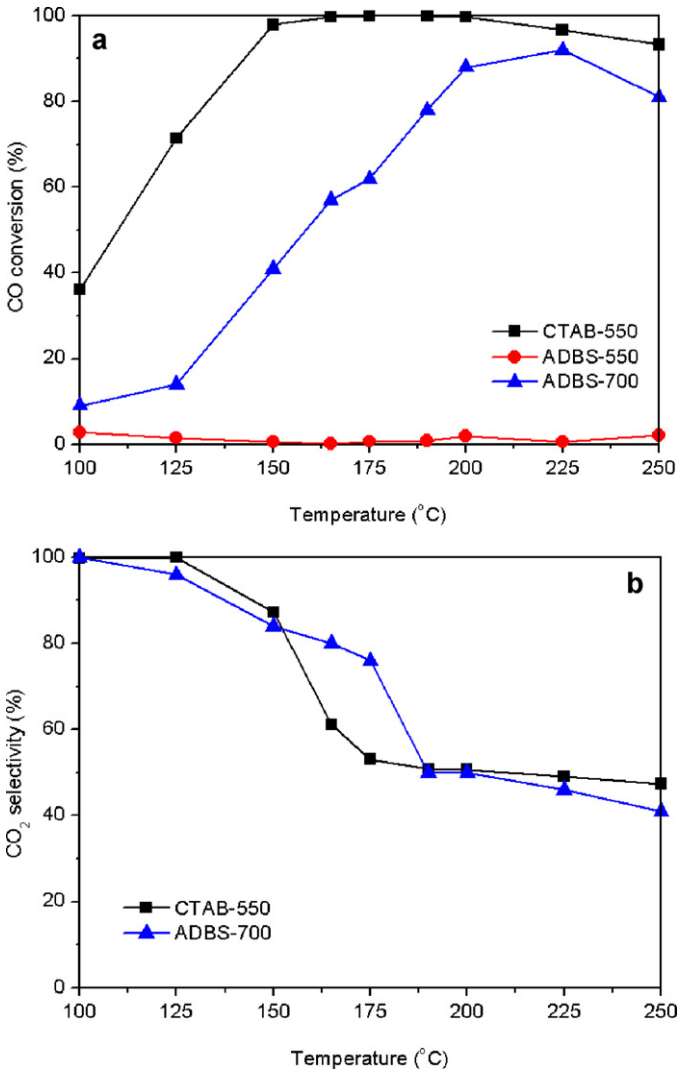

Fig. 1. Catalytic properties of 20 wt.% Co_3O_4/*meso*-$Ce_{0.85}Zr_{0.15}O_2$ catalysts prepared by SACP-IWI method with different SDA for CO PROX, (a) CO conversion; (b) CO_2 selectivity. Operation conditions: GHSV = 15,000 ml h^{-1} g^{-1}, 1 vol.% CO, 1 vol.% O_2, 50 vol.% H_2 and Ar balance.

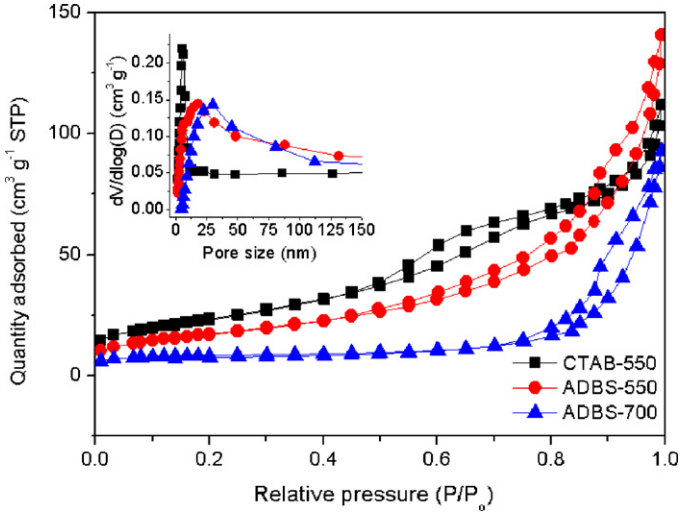

Fig. 2. Nitrogen adsorption/desorption isotherm and pore diameter distribution (inset) of 20 wt.% Co_3O_4/*meso*-$Ce_{0.85}Zr_{0.15}O_2$ catalysts with different SDA.

Table 1
N_2 adsorption/desorption and XRD analysis results for 20 wt.% Co_3O_4/*meso*-$Ce_{0.85}Zr_{0.15}O_2$ catalysts with different SDA.

Sample	BET surface area ($m^2\ g^{-1}$)	Average pore diameter (nm)	Pore volume ($cm^3\ g^{-1}$)	$Ce_{0.85}Zr_{0.15}O_2$		Co_3O_4	
				Crystallite lattice type	Average crystallite size (nm)	Crystallite lattice type	Average crystallite size (nm)
CTAB-550	85.2	6.6	0.14	Fm-3m	6.8	Fd-3m	10.9
ADBS-550	63.0	10.6	0.17	Fm-3m	7.5	Fd-3m	13.9
ADBS-700	29.1	15.2	0.11	Fm-3m	12.6	Fd-3m	17.8

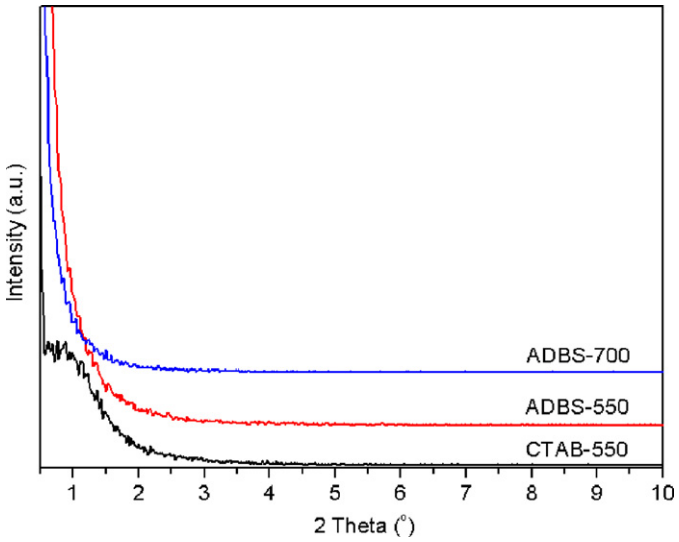

Fig. 3. Small-angle XRD patterns of 20 wt.% Co_3O_4/*meso*-$Ce_{0.85}Zr_{0.15}O_2$ catalysts with different SDA.

From Fig. 2, the N_2 sorption isotherms of the three samples show representative type-IV curves with distinct hysteresis loops, suggesting the mesoporous feature but different pore architecture of the ceria-zirconia prepared with different SDA [34]. From the low-angle XRD patterns of the three catalysts presented in Fig. 3, the CTAB-550 is an ordered mesoporous materials (well-resolved diffraction peaks in the low-angle XRD patterns), while ADBS as template gives rise to less ordered mesopores (no well-resolved diffraction peaks in the low-angle XRD patterns for ADBS-550 and ADBS-700). From wide-angle XRD patterns (Fig. 4), both CTAB and ADBS lead to a fluorite-type cubic $Ce_{0.85}Zr_{0.15}O_2$ composite oxide. The CTAB-550 catalyst, with a crystallite size of 6.8 nm for $Ce_{0.85}Zr_{0.15}O_2$ and 10.9 nm for Co_3O_4 crystalline phases, has a high specific surface area (85.2 $m^2\ g^{-1}$) and a narrow pore diameter distribution. However, the ADBS-550 catalyst only has a lower surface area (63.0 $m^2\ g^{-1}$) but broader pore size distribution, with a crystallite size of 7.5 nm for $Ce_{0.85}Zr_{0.15}O_2$ support and 13.9 nm for Co_3O_4. Thus it might be a reason for distinct catalytic performance in CO PROX reaction. But from Fig. 1, the CO PROX reaction can hardly take place on ADBS-550 catalyst, suggesting that there still exist some other reasons for its unbelievable low catalytic activity, besides the difference in pore architecture, specific surface area and crystallite size of $Ce_{0.85}Zr_{0.15}O_2$ and Co_3O_4. In order to probe into the possible reasons, the ceria-zirconia prepared with ADBS was further calcined before cobalt oxide being supported, so as to remove the possible residual sulfur.

From Figs. 2 and 3 and Table 1, the ADBS-700 exhibits the lower specific surface area (29.1 $m^2\ g^{-1}$) and the larger crystallite size of $Ce_{0.85}Zr_{0.15}O_2$ (12.6 nm) and Co_3O_4 (17.8 nm), but much better catalytic performance for CO PROX reaction, compared with ADBS-550. Generally, the ADBS-700 should have indicated worse catalytic performance than ADBS-550, further implying the inhibition of the residual sulfur towards the catalytic activity for CO PROX reaction. Fig. 5 presents the FT-IR spectra of ADBS-550 and ADBS-700. We can clearly see that the intensity of peak for asymmetric vibration and symmetric stretching vibration of S=O bond (1191 and 1052 cm^{-1}) drop down markedly, inferring the elimination of most residual sulfur while the ceria-zirconia support was further calcined at higher temperature of 700 °C. The NH_3-TPD results in Fig. 6 show that the more acidic sites appear on ADBS-550 than those on ADBS-700. Previous report proved that surface rich acidic and basic sites in equal ratio are required for maximum catalytic performance [35].

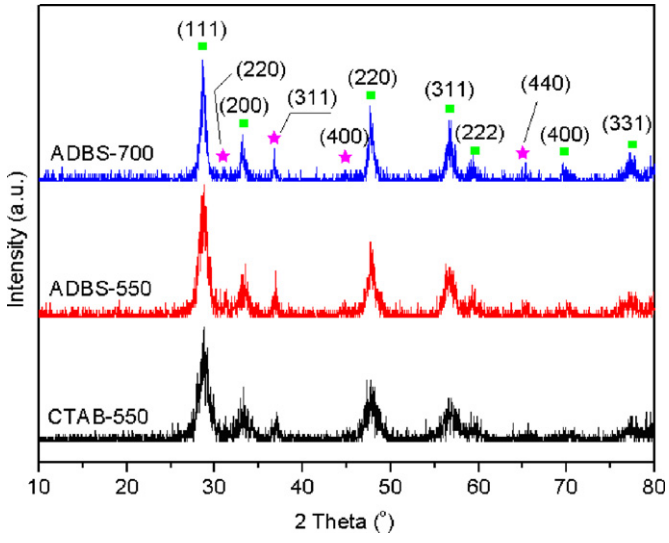

Fig. 4. Wide-angle XRD patterns of 20 wt.% Co_3O_4/*meso*-$Ce_{0.85}Zr_{0.15}O_2$ catalysts with different SDA: (■) fluorite-type cubic $Ce_{0.85}Zr_{0.15}O_2$ composite oxide; (⋆) cubic Co_3O_4.

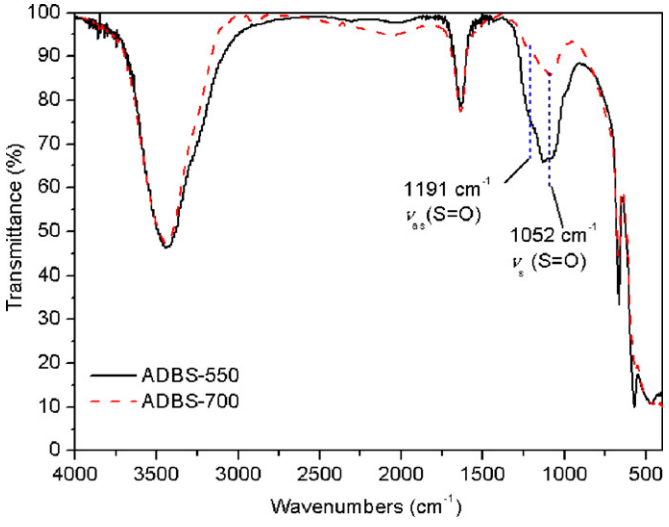

Fig. 5. FTIR spectra of 20 wt.% Co_3O_4/*meso*-$Ce_{0.85}Zr_{0.15}O_2$ catalysts prepared by ADBS with different T_{sup}.

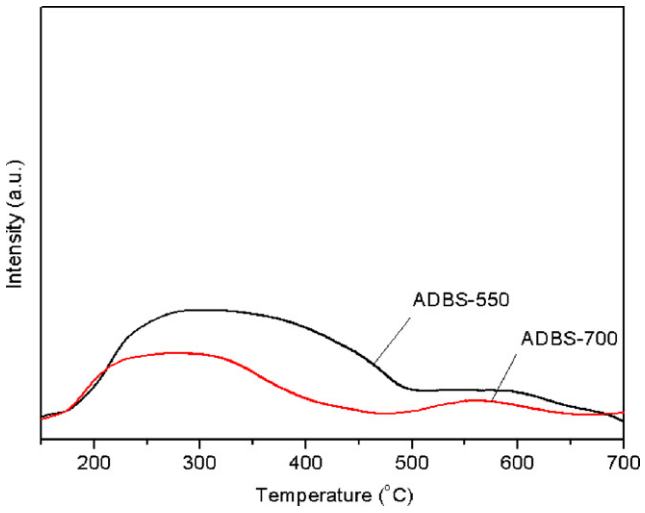

Fig. 6. NH_3-TPD profiles over 20 wt.% Co_3O_4/*meso*-$Ce_{0.85}Zr_{0.15}O_2$ catalysts prepared by ADBS with different T_{sup}.

Unfortunately, the acidic properties of ADBS-550 sample break the equilibrium of the acidic and basic sites. As a result, CO PROX reaction can hardly happen on the ADBS-550 catalyst, but can smoothly take place on ADBS-700, though with the lower specific surface area, the larger crystallite size and worse Co_3O_4 dispersion.

Combining the catalytic properties and the characterization results, it can be safely deduced that the residual sulfur in catalyst is the main factor accounts for the inactivity of ADBS-550. Moreover, in comparison of CTAB-550, the ADBS-700 catalyst indicates worse catalytic performance for CO PROX reaction in excess H_2, which can be contributed to the lower specific surface area, broader pore size distribution, larger crystallite sizes of $Ce_{0.85}Zr_{0.15}O_2$ and Co_3O_4. In all following cases, the *meso*-$Ce_xZr_{1-x}O_2$ composite oxides prepared by SACP method with CTAB as SDA were used to support cobalt oxide for yielding Co_3O_4/*meso*-$Ce_xZr_{1-x}O_2$ catalysts.

3.2. Effect of Ce/(Ce + Zr) atomic ratio

The incorporation of zirconium into CeO_2 lattice is generally beneficial for the improvement of thermal stability of ceria and the mobility of oxygen [36,37]. With an appropriate amount of zirconium being doped, the redox properties of $Ce_xZr_{1-x}O_2$ solid solution might be optimized. The redox behavior of cobalt oxides on the $Ce_xZr_{1-x}O_2$ solid solution might be improved by the metal–support interaction, thus promoting their catalytic activity. It had been revealed that the $Ce_xZr_{1-x}O_2$ composite with a low Zr-content exhibited good oxygen storage capacity and high oxygen mobility [36,38–40]. Our previous studies have also presented the similar results [32]. A series of 20 wt.% Co_3O_4/*meso*-$Ce_xZr_{1-x}O_2$ (x = 1, 0.95, 0.85 and 0.75) catalysts were synthesized by the SACP-IWI method, and the relationship between their redox properties and catalytic performance for CO PROX reaction was studied. Fig. 7 presents the CO conversion and CO_2 selectivity for this reaction over the 20 wt.% Co_3O_4/*meso*-$Ce_xZr_{1-x}O_2$ catalysts with various Ce/(Ce + Zr) atomic ratios.

From Fig. 7, clear difference in catalytic activity has been observed on those catalysts due to the different Ce/(Ce + Zr) atomic ratios. The catalytic activity related to x value rises in the order: $x = 1 < x = 0.75 < x = 0.95 < x = 0.85$. The CO conversion reaches 100% in the temperature range of 165–200 °C over the 20 wt.% Co_3O_4/*meso*-$Ce_{0.85}Zr_{0.15}O_2$, and 175–200 °C over the 20 wt.% Co_3O_4/*meso*-$Ce_{0.95}Zr_{0.05}O_2$. Compared with Co_3O_4/*meso*-$Ce_{0.95}Zr_{0.05}O_2$ catalyst, Co_3O_4/*meso*-$Ce_{0.85}Zr_{0.15}O_2$ exhibited a much higher catalytic activity (the CO conversions over the two

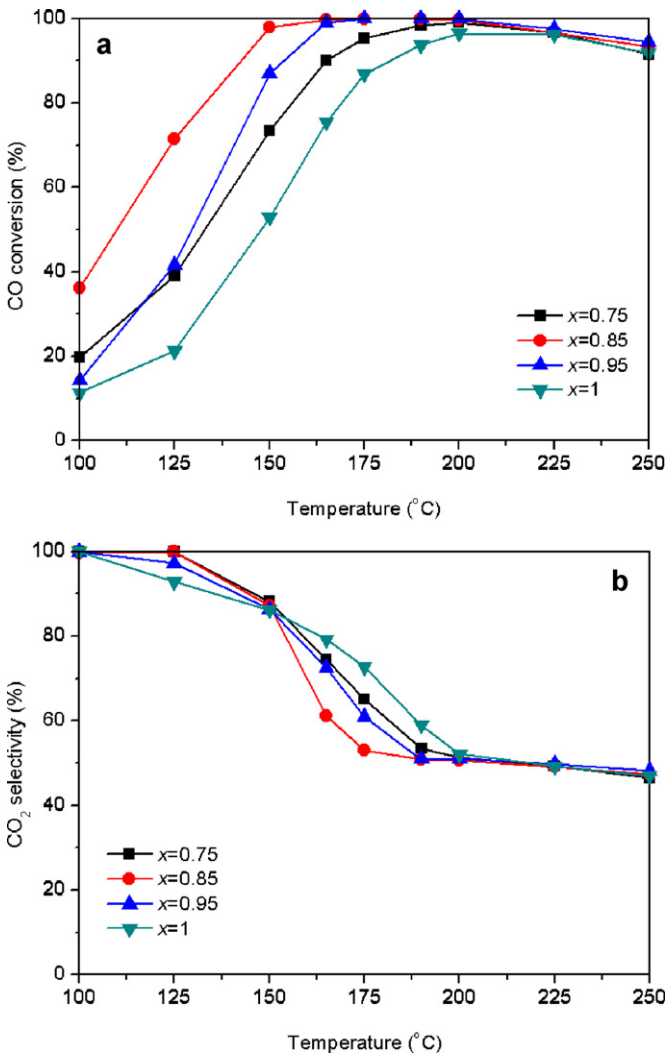

Fig. 7. Effect of Ce/(Ce + Zr) atomic ratio (x) on (a) CO conversion and (b) CO_2 selectivity over the 20 wt.% Co_3O_4/*meso*-$Ce_xZr_{1-x}O_2$ catalysts. Operation conditions: GHSV = 15,000 ml h^{-1} g^{-1}, 1 vol.% CO, 1 vol.% O_2, 50 vol.% H_2 and Ar balance.

catalysts, x = 0.85 and 0.95, are 71.5% and 41.7%, respectively) and a slight higher selectivity (the CO_2 selectivity over the two catalysts, x = 0.85 and 0.95, are 100% and 97.3%, respectively) at lower temperature (125 °C). Furthermore, the same CO conversion of 100% and CO_2 selectivity of 50% over the two catalysts (x = 0.85 and 0.95) can be observed in the temperature range of 190–200 °C.

Generally, the redox behaviors have an inherent relationship with catalytic properties for oxidation reactions. H_2-TPR experiments were performed on 20 wt.% Co_3O_4/*meso*-$Ce_xZr_{1-x}O_2$ (x = 0.75, 0.85, 0.95 and 1) catalysts, the H_2-TPR profiles are plotted in Fig. 8 and the quantitative analysis results are listed in Table 2. The peaks between 240 and 350 °C of catalysts are attributed to the H_2 consumption for the reduction of highly dispersed Co_3O_4 at interface between Co_3O_4 and CeO_2 [31,41]. The smaller crystallite size of active component appears on the ceria-zirconia support with appropriate Ce content [42], resulting in a lower reduction temperature of Co_3O_4. As a result, higher catalytic activity can be obtained. The increase in ZrO_2-doping amount leads to the increase in reducible CeO_2 percentage, suggesting the possible strong interaction between ZrO_2 and CeO_2 can strengthen the mobility of oxygen and promote CeO_2 reduction, which agrees well with the TPR results presented in Fig. 8 and Table 2, and accordingly the catalyst with x = 0.75 should be more active than x = 0.85 and x = 0.95,

Table 2
H_2-TPR quantitative analysis results for 20 wt.% Co_3O_4/*meso*-$Ce_xZr_{1-x}O_2$ with different Ce/(Ce + Zr) atomic ratios (x).

x	Total H_2 uptake (μmol g^{-1})	CeO_2 content (μmol g^{-1})	Reducible CeO_2 content (μmol g^{-1})	Reducible CeO_2 (%)
1	3576	4652	126	2.7
0.95	4292	4480	484	10.8
0.85	4312	4128	494	12.0
0.75	5024	3606	850	23.6

however this is not the case. The unexpected phenomena can be explained as follows: Co_3O_4 is considered to be main active species for CO PROX reaction. The reducible CeO_2 has certain effect on the catalytic properties of ceria-zirconia supported cobalt catalysts, but this effect is not a decisive factor.

Moreover, previous reports showed that the increase in Ce content of support only had a slight influence on the specific surface area of supported catalysts [41–44]. On the basis of the above analysis and discussion, the appropriate Ce/(Ce + Zr) ratio in ceria-zirconia support is required, and the 20 wt.% Co_3O_4/*meso*-$Ce_{0.85}Zr_{0.15}O_2$ catalyst exhibits outstanding catalytic performance for CO PROX reaction.

3.3. Effect of cobalt oxide loading

Our previous report [32] reveals that the $Co_3O_4/Ce_{0.85}Zr_{0.15}O_2$ catalyst synthesized by reverse-microemulsion and subsequent IWI method with ultralow loading (1.8 wt.% Co_3O_4) has been considered as a promising catalyst for CO PROX reaction in excess H_2. The increasing loading of active component in appropriate amount would definitely benefit the CO PROX reaction by providing more active sites. In this study, the effect of cobalt oxide loading of $Co_3O_4/Ce_{0.85}Zr_{0.15}O_2$ on the catalytic performance in CO PROX reaction was investigated. The corresponding reaction results are presented in Fig. 9.

From Fig. 9, Co_3O_4/*meso*-$Ce_{0.85}Zr_{0.15}O_2$ catalysts with various cobalt loadings exhibit satisfactory catalytic properties for CO PROX reaction in H_2-rich gases. Complete CO conversion and similar CO_2 selectivity have been achieved over the supported cobalt oxide catalysts with a wide loading range in 16–27 wt.% at the temperature of 165–200 °C. But the further increase in reaction temperature from 200 to 250 °C leads to the decrease in CO conversion, due to the competitive oxidation reactions between CO and H_2. Reacting with H_2 leads to insufficient amount of oxygen left for CO complete oxidation. The change in cobalt loading significantly affects both the CO conversion and CO_2 selectivity at lower temperature. With the cobalt oxide loading being increased from 4 to 20 wt.%, the activity for CO PROX reaction is improved meanwhile, and the maximum CO conversion and CO_2 selectivity at low temperature region (100–165 °C) are obtained on the supported cobalt oxide catalyst with 20 wt.% loading. Nevertheless, the decrease in both CO conversion and CO_2 selectivity can be observed while the cobalt oxide loading is further increased from 20 to 27 wt.%. The larger loading leads to the decrease in specific surface area [43,45], which is detrimental to the catalytic performance of supported cobalt oxide catalyst. Therefore, the 20 wt.% of appropriate cobalt oxide loading is required for CO PROX reaction.

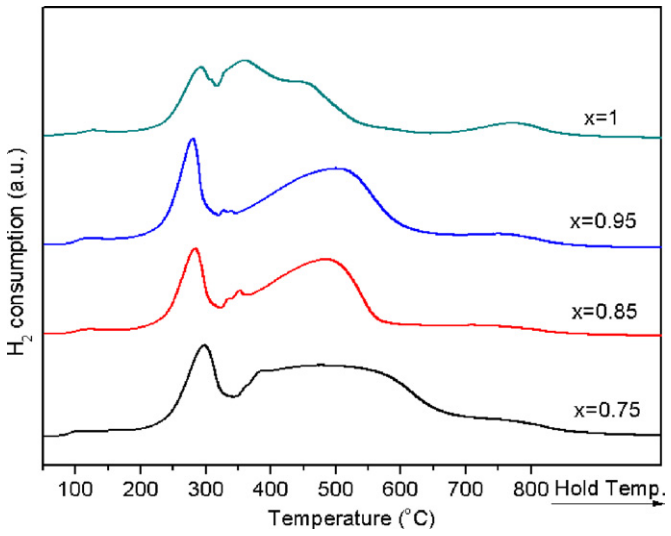

Fig. 8. H_2-TPR profiles of 20 wt.% Co_3O_4/*meso*-$Ce_xZr_{1-x}O_2$ catalysts with various Ce/(Ce + Zr) atomic ratios.

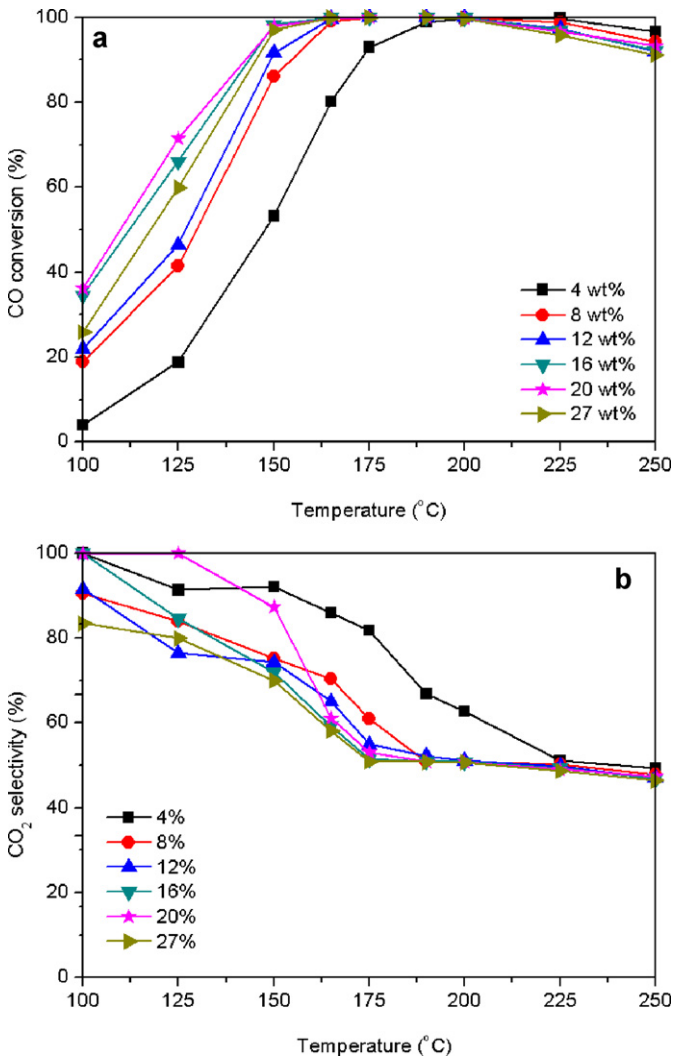

Fig. 9. Effect of Co_3O_4 loadings on (a) CO conversion and (b) CO_2 selectivity over the Co_3O_4/*meso*-$Ce_{0.85}Zr_{0.15}O_2$ catalysts. Operation conditions: GHSV = 15,000 ml h^{-1} g^{-1}, 1 vol.% CO, 1 vol.% O_2, 50 vol.% H_2 and Ar balance.

Table 3
H_2-TPR quantitative analysis results for the Co_3O_4/*meso*-$Ce_{0.85}Zr_{0.15}O_2$ catalysts with a loading range in 4–27 wt.%.

Sample	H_2 uptake (μmol g^{-1})	α (°C)	β (°C	γ (°C)	γ' (°C)	δ (°C)	H_2 uptake for Co_3O_4 (μmol g^{-1})	H_2 uptake for CeO_2 (μmol g^{-1})
4 wt.% $Co_3O_4/Ce_{0.85}Zr_{0.15}O_2$	2736	97	268	345	366	485	664	1616
8 wt.% $Co_3O_4/Ce_{0.85}Zr_{0.15}O_2$	2900	99	269	336	353	485	1328	1572
12 wt.% $Co_3O_4/Ce_{0.85}Zr_{0.15}O_2$	3192	82	276	335	353	478	1994	1198
16 wt.% $Co_3O_4/Ce_{0.85}Zr_{0.15}O_2$	3704	119	279	334	352	496	2658	1046
20 wt.% $Co_3O_4/Ce_{0.85}Zr_{0.15}O_2$	4312	117	283	332	352	492	3324	988
27 wt.% $Co_3O_4/Ce_{0.85}Zr_{0.15}O_2$	4890	113	286	338	349	483	4486	404

H_2-TPR experiments were also performed on 4–27 wt.% Co_3O_4/*meso*-$Ce_{0.85}Zr_{0.15}O_2$ catalysts to investigate the reducibility and metal–support interaction on catalysts with various cobalt loadings. The H_2-TPR profiles are shown in Fig. 10, with quantitative analysis results presented in Table 3.

On the basis of previous reports [46], we assign the peaks at about 100 °C (denoted as α-peak) to the reduction of highly dispersed Co_3O_4 over the support. Luo et al. [31] pointed out that reduction of fine particles of Co_3O_4 went into two steps: $Co_3O_4 \rightarrow CoO \rightarrow Co$. It is generally accepted that the Zr^{4+} is an unreducible ion, and thus the H_2 consumption mainly due to the reduction of Co_3O_4 and CeO_2, among which Co_3O_4 is believed to be reduced below 400 °C [28]. There are three or four reduction peaks (denoted as β, γ, γ' and δ) in the temperature range 200–500 °C for all samples. The β-peak is ascribed to the reduction of Co^{3+} to Co^{2+}, while the δ-peak is associated with the reduction of Co^{2+} as well as of Ce^{4+} [36,47]. The interaction between support and cobalt makes the H_2-TPR profile into a more complex one [28,48], and therefore the two peaks (γ and γ') attributed to reduction of cobalt oxide appear on the TPR profiles of ceria-zirconia supported cobalt oxide catalysts. As cobalt oxide loading is increased, the increasing amount of H_2 is consumed and the β and δ peak shifted to higher temperatures, which can be ascribed to the agglomeration of cobalt oxides and the possible metal–support interaction. From the H_2-TPR profiles of the series of supported cobalt oxide catalysts with various loadings from 4 to 27 wt.%, both the total H_2 uptake and Co_3O_4 H_2 uptake increase, but the CO conversion does not follow this trend and 20% is the optimum loading. The unexpected reaction results might be ascribed to decrease in specific surface area of catalysts, the increase in crystallite size of Co_3O_4 ascribed to agglomeration and also the shift of reduction peaks to higher temperature, which would be further investigated as follows.

The XRD patterns of Co_3O_4/*meso*-$Ce_{0.85}Zr_{0.15}O_2$ catalysts with various cobalt oxide loadings are shown in Fig. 11, and the quantitative analysis results are listed in Table 4. Pure cubic phase of $Ce_{0.85}Zr_{0.15}O_2$ according to (111), (200), (220) and (311) are identified on the basis of previous reports [43,49,50] and JCPDS file (28-0271) of the $Ce_{0.75}Zr_{0.25}O_2$. No diffraction peaks of pure CeO_2 or ZrO_2 phases are detected for all Co_3O_4/*meso*-$Ce_{0.85}Zr_{0.15}O_2$ catalysts, implying no phase separation of the samples [32], which is consistent with results in previous section for catalysts prepared by ADBS (Fig. 3). The crystallite size of $Ce_{0.85}Zr_{0.15}O_2$ solid solution is not obviously affected by cobalt loading (6.2–6.8 nm). The cubic phase Co_3O_4 with the Fd-3m crystallite type is identified in comparison with the corresponding JCPDS file (43-1003). The characteristic peaks for Co_3O_4 are not visible until the loading reach up to 8 wt.%, and the sharpened diffraction peaks of Co_3O_4 could be observed as loading further grows, suggesting the growth of crystallite size (from 7.2 to 11.8 nm) resulted from the agglomeration of cobalt oxide, which is in agreement with the previous report [43].

From the above, the increase in loading can yield more active sites, which is beneficial for catalytic performance. However, it can also lead to the decrease in specific surface area of catalysts, the increase in crystallite size of Co_3O_4 ascribed to agglomeration and the shift of reduction peaks to higher temperature. As a result, the catalytic activity for CO PROX reaction on $Co_3O_4/Ce_{0.85}Zr_{0.15}O_2$ increases along with the increasing cobalt loading. However, as the loading exceeds 20 wt.%, both the CO conversion and the CO_2 selectivity decrease. The appropriate cobalt oxide loading is required.

3.4. *Effect of adding H_2O and CO_2*

The hydrogen-rich stream coming from reforming gases, usually, contains a certain amount of CO_2 and H_2O. Thus, the study on

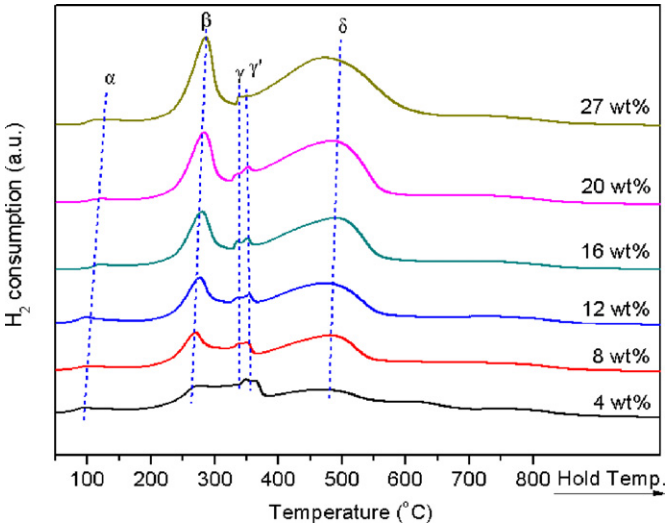

Fig. 10. H_2-TPR profiles of Co_3O_4/*meso*-$Ce_{0.85}Zr_{0.15}O_2$ catalysts with various Co_3O_4 loadings.

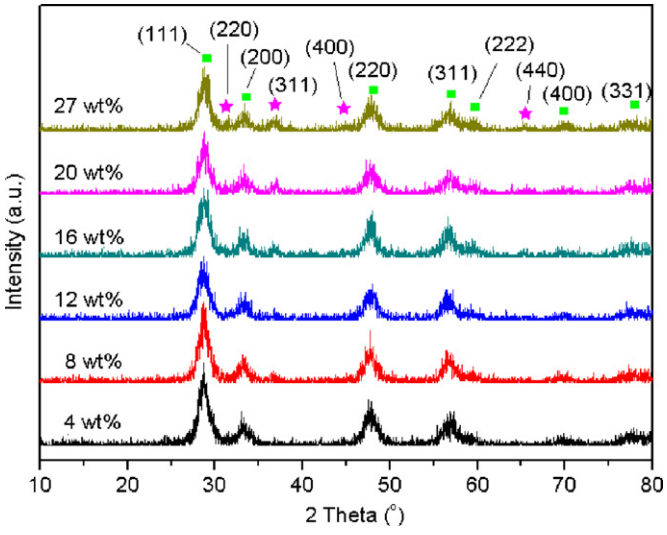

Fig. 11. XRD patterns of Co_3O_4/*meso*-$Ce_{0.85}Zr_{0.15}O_2$ catalysts with various Co_3O_4 loadings: (■) fluorite-type cubic $Ce_{0.85}Zr_{0.15}O_2$ composite oxide; (★) cubic Co_3O_4.

Table 4
XRD analysis results for Co_3O_4/*meso*-$Ce_{0.85}Zr_{0.15}O_2$ catalysts with different cobalt oxide loadings.

Cobalt loading (wt.%)	$Ce_{0.85}Zr_{0.15}O_2$		Co_3O_4	
	Crystallite lattice type	Average crystallite size (nm)	Crystallite lattice type	Average crystallite size (nm)
4	Fm-3m	6.2	–	–
8	Fm-3m	6.2	Fd-3m	7.2
12	Fm-3m Fm-3m	6.2	Fd-3m	9.6
16	Fm-3m	6.4	Fd-3m	10.4
20	Fm-3m	6.8	Fd-3m	10.9
27		6.5	Fd-3m	11.8

catalytic performance of catalysts for CO PROX reaction with CO_2 and H_2O in feed gas is of great significance. The effect of adding CO_2 and H_2O to feed gas on catalytic properties over our developed Co_3O_4/*meso*-$Ce_{0.85}Zr_{0.15}O_2$ catalyst was investigated. Fig. 12 provides the reaction results.

From Fig. 12(a), the existence of 10 vol.% H_2O or 10 vol.% CO_2 has a similar negative effect on catalytic activity of 20 wt.% Co_3O_4/*meso*-$Ce_{0.85}Zr_{0.15}O_2$ catalyst for CO PROX reaction. Almost complete CO removal can only happen at the temperature range 190–200 °C, much narrower than that without H_2O or CO_2. However, with adding both CO_2 and H_2O, the CO conversion can only reach 96.1% at 225 °C, which is higher than those in previous report about the CO PROX reactions over the CuO/$Ce_{1-x}Zr_xO_2$ catalyst [51]. From Fig. 12(b), the CO_2 selectivity rises in the following order: without (CO_2 + H_2O) < with CO_2 < with H_2O < with CO_2 + H_2O. The negative effect of H_2O can be attributed to the blockage of the active sites on the surface of catalyst by the adsorbed water [51,52]. The negative influence of adding CO_2 on catalytic performance can be contributed to the following different aspects. On the one hand, it may be ascribed to the competitive adsorption of CO and CO_2 on the surface of catalyst [51]; On the other hand, the previous reports [52,53] proposed that the Co^{2+} ions coming from the reduction of Co^{3+} during the CO PROX reaction process tend to be occupied by CO_2 and become difficult to be re-oxidized. The formation of

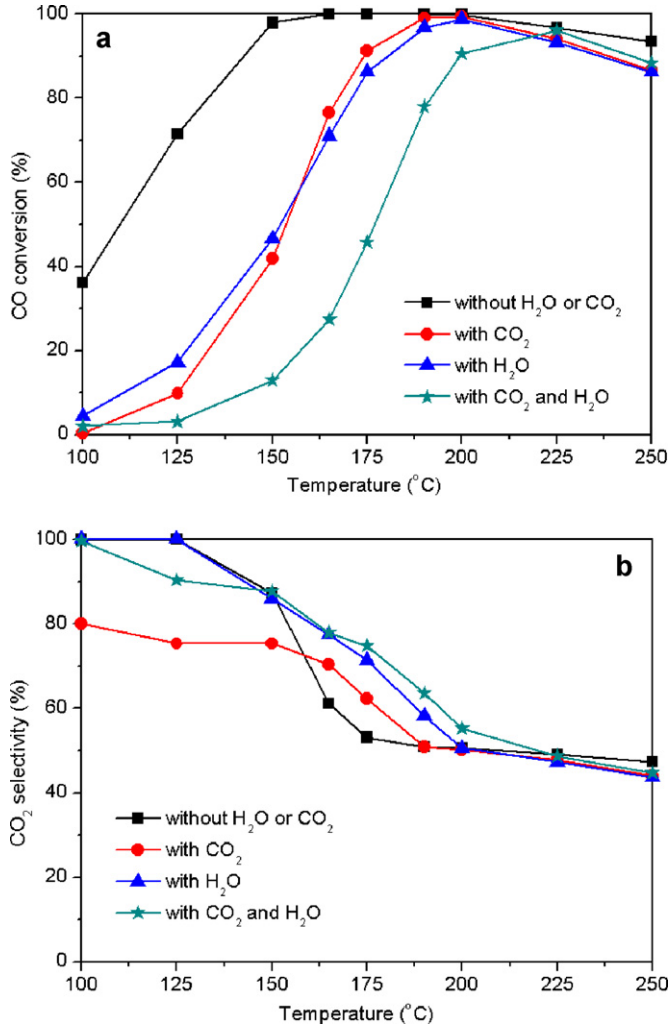

Fig. 12. CO conversion (a) and CO_2 selectivity (b) in the presence of CO_2 and H_2O. Reaction conditions: 1.0% O_2, 1.0% CO, 50% H_2, 10% CO_2 or/and 10% H_2O and Ar balance; GHSV = 15,000 ml g^{-1} h^{-1}.

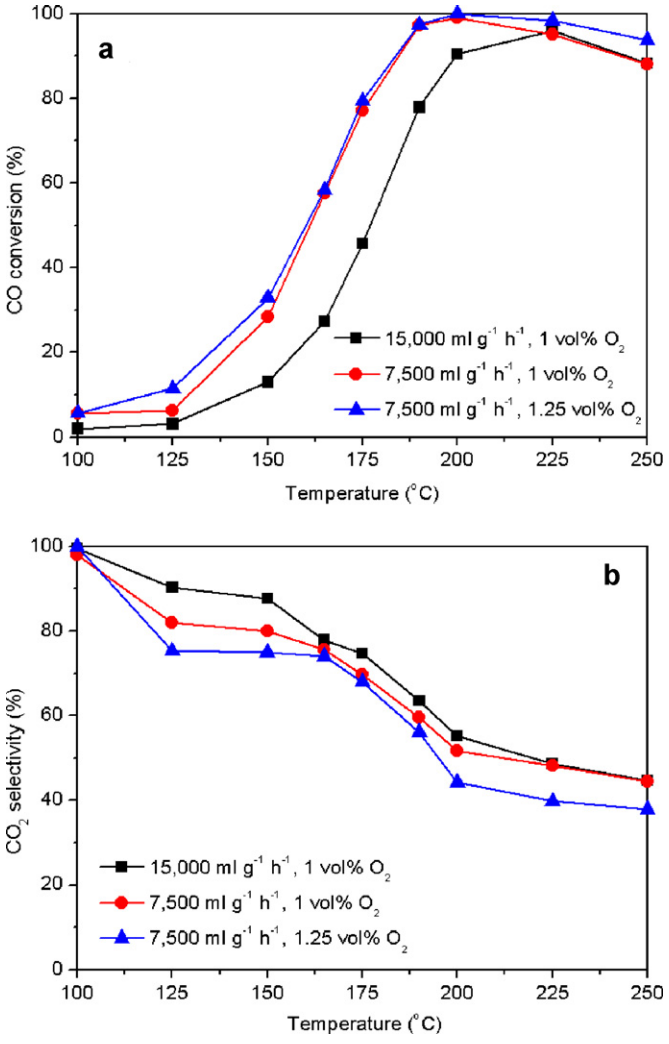

Fig. 13. Effects of GHSV and O_2 concentration on (a) CO conversion and (b) CO_2 selectivity. Operation conditions: GHSV = 15,000 or 7500 ml h^{-1} g^{-1}, 1 or 1.25 vol.% O_2, 1 vol.% CO, 10 vol.% H_2O, 10 vol.% CO_2, 50 vol.% H_2 and Ar balance.

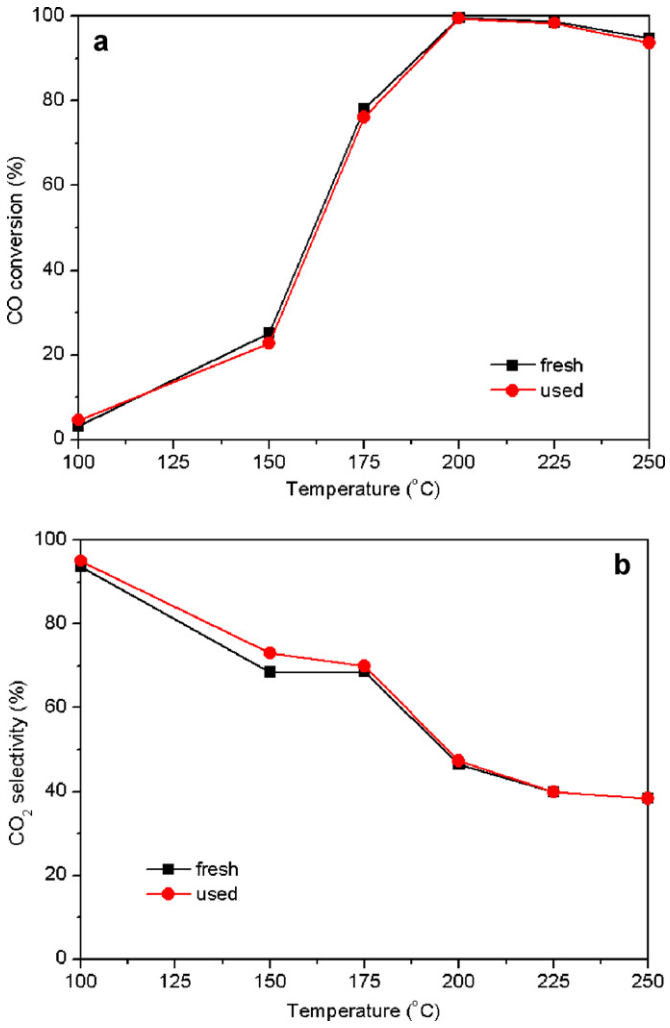

Fig. 14. CO conversion (a) and CO_2 selectivity (b) in the presence of CO_2 and H_2O on the fresh and used 20 wt.% Co_3O_4/*meso*-$Ce_{0.85}Ze_{0.15}O_2$ catalyst. Reaction conditions: 1.25 vol.% O_2, 1.0 vol.% CO, 50 vol.% H_2, 10 vol.% CO_2 and 10 vol.% H_2O and Ar balance; GHSV = 7500 ml g^{-1} h^{-1}.

specific cobalt carbonate breaks the redox circle, resulting in the lower catalytic activity. In addition, the reverse WGS reaction may also lower the overall CO conversion by adding CO_2 in the H_2-rich stream at high temperature.

3.5. Effect of GHSV and O_2 concentration

The 20 wt.% Co_3O_4/*meso*-$Ce_{0.85}Zr_{0.15}O_2$ was chosen to investigate the effects of GHSV and O_2 concentration on the catalytic properties for CO PROX reaction in the presence of CO_2 and H_2O. The reaction results were illustrated in Fig. 13.

From Fig. 13(a), the CO conversion increases at the given temperatures as the decrease in the GHSV from 15,000 to 7500 ml g^{-1} h^{-1}. At 7500 ml g^{-1} h^{-1}, the CO conversion reaches 100% at 200 °C, while the CO conversion is about 90.5% at 15,000 ml g^{-1} h^{-1}. The CO conversion can be increased by extending the contact time of the catalyst with the feed. From Fig. 13(b), the similar selectivity of O_2 to CO oxidation for these two different GHSV can be observed.

In order to reveal whether the further increased O_2 concentration can improve the reaction performance or not, the CO PROX reactions were performed over 20 wt.% Co_3O_4/*meso*-$Ce_{0.85}Zr_{0.15}O_2$ by varying the O_2 concentration from 1.0 to 1.25 vol.% in the presence of CO_2 and H_2O at 7500 ml g^{-1} h^{-1} GHSV. From Fig. 13, with 1.0 vol.% O_2 in the feed, the CO conversion can reach almost 100% at 200 °C. Further increasing O_2 concentration from 1.0 to 1.25 vol.%, CO can be fully converted at 200 °C, though with a slight decrease in CO_2 selectivity. At the higher reaction temperature region (above 200 °C), the higher O_2 concentration can result in higher CO conversion, which can be contributed to the more O_2 supplied for CO oxidation transformation in competition with H_2 oxidation.

3.6. Stability of developed catalyst for CO PROX reaction

The stability of the 20 wt.% Co_3O_4/*meso*-$Ce_{0.85}Zr_{0.15}O_2$ catalyst was investigated by performing a second run over the used sample. The reaction results over the fresh and used catalysts are presented in Fig. 14. As can be seen, the developed catalyst exhibits excellent catalytic stability. In comparison with the fresh catalyst, the used one exhibits a similar good catalytic activity and a little higher selectivity, suggesting the developed 20 wt.% Co_3O_4/*meso*-$Ce_{0.85}Zr_{0.15}O_2$ catalyst prepared by SACP-IWI method be a robust and effective catalyst for CO PROX reaction to eliminate the trace CO from H_2-rich stream.

4. Conclusions

A series of mesoporous Co_3O_4/$Ce_xZr_{1-x}O_2$ catalysts were synthesized by SACP-IWI method. Employing CTAB as SDA, the prepared catalysts possess order mesoporous architecture and show promising catalytic performance for CO PROX reaction in excess H_2. However, the supported cobalt oxide catalyst with ceria-zirconia as support prepared by SACP method using the ADBS as SDA owns much worse activity for CO PROX reaction. From the analysis results of NH_3-TPD and FTIR, the negative effect of anionic ADBS as SDA can be mainly corroborated to the residual sulfur, which gives an acidic nature to catalyst that is apt to break the equilibrium of surface acidic and basic sites, resulting in very low activity for CO oxidation. The ordered mesoporous ceria-zirconia composite oxide prepared by SACP method with CTAB as SDA is an appropriate support for preparing supported cobalt oxide catalyst for CO PROX reaction in excess H_2. Results showed that the appropriate Ce/(Ce + Zr) ratio in ceria-zirconia support and cobalt oxide loading are required, and the 20 wt.% Co_3O_4/*meso*-$Ce_{0.85}Zr_{0.15}O_2$ catalyst exhibits outstanding catalytic performance for CO PROX reaction. Co_3O_4 is considered to be main active species for CO PROX reaction, while the impact of reducible CeO_2 also cannot be neglected. In a word, the prepared Co_3O_4/*meso*-$Ce_xZr_{1-x}O_2$ (CTAB as SDA) could be effective catalysts for eliminating CO from H_2-rich gases, and the catalytic performance is dependent on the redox behavior and Co_3O_4 dispersion, affected by the Ce/(Ce + Zr) ratio and cobalt oxide loading.

Acknowledgements

This work is financially supported by the National Natural Science Foundation of China (no. 20803006) and the Fundamental Research Funds for the Central Universities.

References

[1] P.F. Zhu, J. Li, S.F. Zuo, R.X. Zhou, Appl. Surf. Sci. 255 (2008) 2903–2909.
[2] E. Moretti, L. Storaro, A. Talon, M. Lenarda, Catal. Commun. 10 (2009) 522–527.
[3] Y. Zhang, H. Liang, X.Y. Gao, Y. Liu, Catal. Commun. 10 (2009) 1432–1436.
[4] D. Gamarra, G. Munuera, A.B. Hungría, M. Fernández-García, J.C. Conesa, P.A. Midgley, X.Q. Wang, J.C. Hanson, J.A. Rodríguez, A. Martínez-Arias, J. Phys. Chem. C 111 (2007) 11026–11038.
[5] J.L. Ayastuy, M.A. Gutiérrez-Ortiz, J.A. González-Marcos, A. Aranzabal, J.R. González-Celasco, Ind. Eng. Chem. Res. 44 (2005) 41–45.
[6] D.L. Trimm, Z.I. Onsan, Catal. Rev. Sci. Eng. 43 (2001) 31–84.
[7] A. Sirijaruphan, J.G. Goodwin Jr., R.W. Rice, J. Catal. 224 (2004) 304–313.
[8] V. Sebastian, S. Irusta, R. Mallada, J. Santanaría, Appl. Catal. A: Gen. 366 (2009) 242–251.

[9] C.T. Chang, B.J. Liaw, Y.P. Chen, Y.Z. Chen, J. Mol. Catal. A: Chem. 300 (2009) 80–88.
[10] N. Iwasa, S. Arai, M. Arai, Appl. Catal. B: Environ. 79 (2008) 132–141.
[11] F. Arena, P. Famulari, N. Interdonato, G. Bonura, F. Frusteri, L. Spadaro, Catal. Today 116 (2006) 384–390.
[12] A. Atalik, D. Uner, J. Catal. 241 (2006) 268–275.
[13] C.G. Maciel, M.N. Belgacem, J.M. Assaf, Catal. Lett. 141 (2011) 316–321.
[14] C.S. Polster, H. Nair, C.D. Baertsch, J. Catal. 266 (2009) 308–319.
[15] G. Avgouropoulos, T. Ioannides, H. Matralis, Appl. Catal. B: Environ. 56 (2005) 87–93.
[16] J. Han, H.J. Kim, S. Yoon, H. Lee, J. Mol. Catal. A: Chem. 335 (2011) 82–88.
[17] D. Gamarra, A. Martínez-Arias, J. Catal. 263 (2009) 189–195.
[18] Y. Teng, H. Sakurai, A. Ueda, T. Kobayashi, Int. J. Hydrogen Energy 24 (1999) 355–358.
[19] M. Kang, M.W. Song, C.H. Lee, Appl. Catal. A: Gen. 251 (2003) 143–156.
[20] J. Jansson, A.E.C. Palmqvist, E. Fridell, M. Skoglundh, L. Österlund, P. Thormählen, V. Langer, J. Catal. 211 (2002) 387–397.
[21] X.W. Xie, Y. Li, Z.Q. Liu, M. Haruta, W.J. Shen, Nature 458 (2009) 746–749.
[22] M.J. Pollard, B.A. Weinstock, T.E. Bitterwolf, P.R. Griffiths, A.P. Newbery, J.B. Paine, J. Catal. 254 (2008) 218–225.
[23] G.G. Xia, Y.G. Yin, W.S. Willis, J.Y. Wang, S.L. Suib, J. Catal. 185 (1999) 91–105.
[24] P. Broqvist, I. Panas, H. Persson, J. Catal. 210 (2002) 198–206.
[25] K. Omata, Y. Kobayashi, M. Yamada, Catal. Commun. 6 (2005) 563–567.
[26] S. Ozkara, A.N. Akin, Z. Misirli, A.E. Aksoylu, Turk. J. Chem. 29 (2005) 219–224.
[27] M.P. Woods, P. Gawade, B. Tan, U.S. Ozkan, Appl. Catal. B: Environ. 97 (2010) 28–35.
[28] L.F. Liotta, G.D. Carlo, G. Pantaleo, G. Deganello, Catal. Commun. 6 (2005) 329–336.
[29] V.G. Milt, M.A. Ulla, E.A. Lombardo, J. Catal. 200 (2001) 241–249.
[30] C.Y. Lu, M.Y. Wey, Fuel 86 (2007) 1153–1161.
[31] J.Y. Luo, M. Meng, X. Li, X.G. Li, Y.Q. Zha, T.D. Hu, Y.N. Xie, J. Zhang, J. Catal. 254 (2008) 310–324.
[32] Z.K. Zhao, X.L. Lin, R.H. Jin, Y.T. Dai, G.R. Wang, Catal. Commun. 12 (2011) 1448–1451.
[33] A. Aslani, Phys. B 406 (2011) 150–154.
[34] M. Teng, L. Luo, X. Yang, Micropor. Mesopor. Mater. 119 (2009) 158–164.
[35] A.V. Salker, S.J. Naik, Appl. Catal. B: Environ. 89 (2009) 246–254.
[36] S.S.Y. Lin, D.H. Kim, M.H. Engelhard, S.Y. Ha, J. Catal. 273 (2010) 229–235.
[37] S.S.Y. Lin, H. Daimon, S.Y. Ha, Appl. Catal. A: Gen. 366 (2009) 252–261.
[38] G.F. Li, Q.Y. Wang, B. Zhao, R.X. Zhou, J. Mol. Catal. A: Chem. 326 (2010) 69–74.
[39] N. Wang, W. Chu, L.Q. Huang, T. Zhang, J. Nat. Gas Chem. 19 (2010) 117–122.
[40] A.I. Kozlov, D.H. Kim, A. Yezerets, P. Andersen, H.H. Kung, M.C. Kung, J. Catal. 209 (2002) 417–426.
[41] X.L. Tang, B.C. Zhang, Y. Li, Y.D. Xu, Q. Xin, W.J. Shen, Catal. Today 93–95 (2004) 191–198.
[42] S. Damyanova, B. Pawelec, K. Arishtirova, M.V. Martinez Huerta, J.L.G. Fierro, Appl. Catal. B: Environ. 89 (2009) 149–159.
[43] P. Biswas, D. Kunzru, Int. J. Hydrogen Energy 32 (2007) 969–980.
[44] S. Damyanova, B. Pawelec, K. Arishtirova, M.V. Martinez Huerta, J.L.G. Fierro, Appl. Catal. A: Gen. 337 (2008) 86–96.
[45] J.-L. Cao, Y. Wang, T.-Y. Zhang, S.-H. Wu, Z.-Y. Yuan, Appl. Catal. B: Environ. 78 (2008) 120–128.
[46] J.L. Ayastuy, A. Gurbani, M.P. González-Marcos, M.A. Gutiérrez-Ortiz, Appl. Catal. A: Gen. 387 (2010) 119–128.
[47] L.F. Liotta, G.D. Carlo, G. Pantaleo, G. Deganello, Appl. Catal. B: Environ. 70 (2007) 314–322.
[48] Z.K. Zhao, M.M. Yung, U.S. Ozkan, Catal. Commun. 9 (2008) 1465–1471.
[49] A. Martínez-Arias, A.B. Hungría, M. Fernández-García, J.C. Conesa, G. Munuera, J. Power Sources 151 (2005) 32–42.
[50] R. Si, Y.W. Zhang, S.J. Li, B.X. Lin, C.H. Yan, J. Phys. Chem. B 108 (2004) 12481–12488.
[51] J.W. Park, J.H. Jeong, W.L. Yoon, Y.W. Rhee, J. Power Sources 132 (2004) 18–28.
[52] D. Ganarra, A. Martínez-Arias, J. Catal. 263 (2009) 189–195.
[53] Q. Guo, S.Q. Chen, Y. Liu, Y.Q. Wang, Chem. Eng. J. 165 (2010) 846–850.